`

Supporting information for

Oxidatively Stable Ferrocenyl-π-bridge-Titanocene D-π-A Complexes: An Electrochemical and Spectroscopic Investigation of the Mixed-Valence States

Jared A. Pienkos,[a] Alex B. Webster,[a] Eric J. Piechota,[b] A. Danai Agakidou,[a] Colin D. McMillen,[c] David Y. Pritchett,[a] Gerald J. Meyer,[b] and Paul S. Wagenknecht.*[a]

[a]Department of Chemistry, Furman University, Greenville, SC, 29613, USA. [b]Department of Chemistry, The University of North Carolina at Chapel Hill, Chapel Hill, NC, 27599, USA. [c]Department of Chemistry, Clemson University, Clemson, SC, 29634, USA.

`

X-ray Crystallography. Single crystals of $Cp_2Ti(C_2Fc)_2CuBr$ suitable for diffraction were grown as the toluene solvate, from diffusion of hexanes into a toluene solution treated with TEA (1 drop). Single crystals of $Cp^*_2Ti(C_2Fc)_2CuBr$ suitable for diffraction were grown from diffusion of hexanes into a benzene solution treated with TEA (1 drop). The crystal structures were determined by single crystal X-ray diffraction measured using a Bruker D8 Venture diffractometer. Crystals were mounted on a low-scatter loop using paratone, and immediately cooled to 173 ± 2 K in a cold nitrogen gas stream. Data were collected by phi and omega scans using Mo Kα (λ = 0.71073 Å) radiation from an Incoatec microfocus source, and measured by a Photon 100 detector. Data were processed and scaled (multi-scan absorption correction) using the SAINT and SADABS routines in the Apex3 software suite.[1] The space groups were determined based on the systematic absences, and the structures were solved by intrinsic phasing (SHELXT) and subsequently refined by Fourier difference techniques using full-matrix-least-squares on F^2 (SHELXL) using the SHELXTL package.[2] All non-hydrogen atoms were refined anisortropically. Hydrogen atoms attached to carbon atoms were placed in geometrically idealized positions and refined using appropriate riding models.

Details of the data collection and refinements are summarized in Table S1. In addition to the thermal ellipsoid plots in the manuscript, a comparison of the molecular geometries, as well as additional packing diagrams are included as Figures S1-S3 here in the Supporting Information.

`

Table S1: Crystallographic data for $Cp_2Ti(C_2Fc)_2CuBr$ and $Cp^*_2Ti(C_2Fc)_2CuBr$

	$Cp_2Ti(C_2Fc)_2CuBr$	$Cp^*_2Ti(C_2Fc)_2CuBr$
CCDC reference no.	1852310	1852311
Formula	$C_{34}H_{28}BrCuFe_2Ti \cdot C_7H_8$	$C_{44}H_{48}BrCuFe_2Ti$
Formula weight (g/mol)	831.75	879.87
Temperature (K)	173(2)	173(2)
Wavelength (Å)	0.71073	0.71073
Crystal system, space group	monoclinic, $P2_1/c$	monoclinic, $P2_1/c$
a, Å	7.6947(6)	13.9631(19)
b, Å	18.5105(11)	11.5467(13)
c, Å	23.9218(17)	23.644(3)
β, º	98.907(3)	98.371(5)
V, Å^3	3366.2(4)	3771.5(8)
Z, D_{cal} g/cm^3	4, 1.641	4, 1.550
μ, mm^{-1}	2.913	2.604
F(000)	1680	1800
Crystal size, mm	0.30 x 0.21 x 0.03	0.44 x 0.21 x 0.15
Theta range for data	2.36-26.00	2.38-27.00
Reflections collected	50253	115324
Independent reflections	6630	8224
Rint	0.0620	0.0527
Max. and min. transmission	1.0000, 0.7571	1.0000, 0.6234
Data / restraints / param.	6630 / 0 / 416	8224 / 0 / 452
Goodness-of-fit on F^2	1.033	1.046
Final R indices [I>2 σ(I)]	R = 0.0311 wR = 0.0670	R = 0.0342 wR = 0.0882
R indices (all data)	R = 0.0421 wR = 0.0712	R = 0.0421 wR = 0.0929
Largest diff. peak/hole (e·Å^{-3})	0.382/-0.665	0.664/-1.444

`

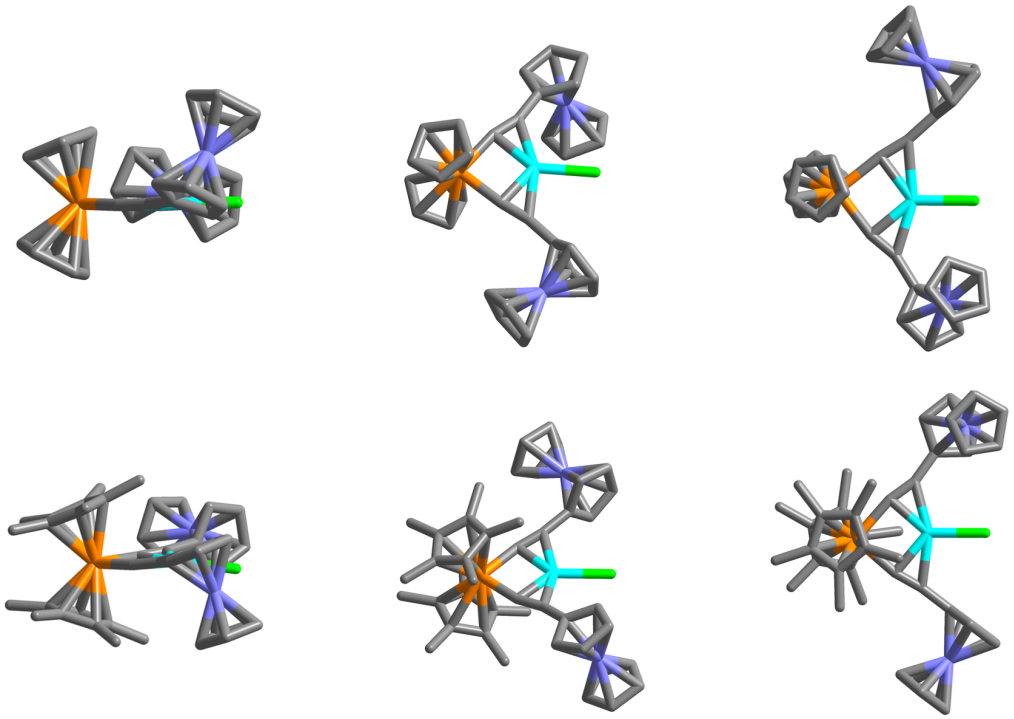

Figure S1: Comparison of three different orientations of $Cp_2Ti(C_2Fc)_2CuBr$ and $Cp^*_2Ti(C_2Fc)_2CuBr$.

`

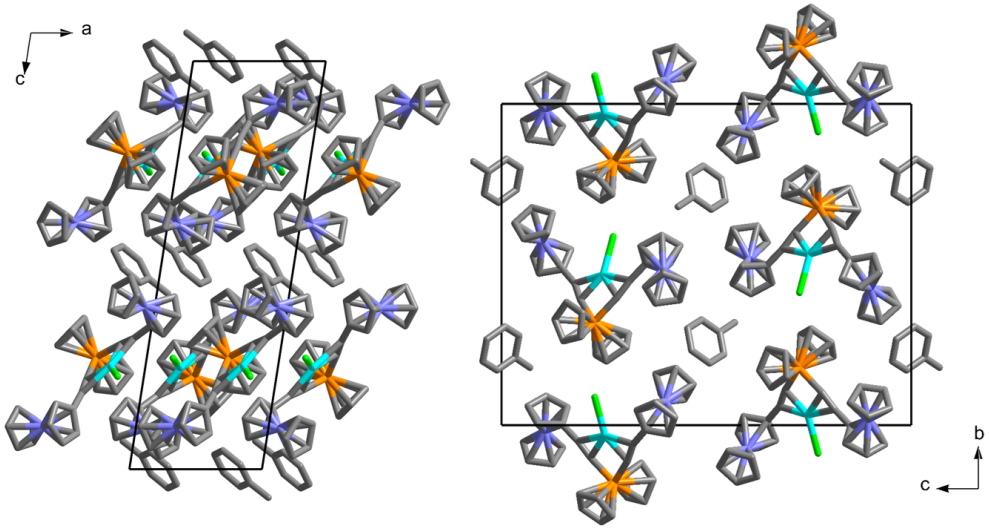

Figure S2: Packing arrangement of $Cp_2Ti(C_2Fc)_2CuBr$ along [010] (left) and [100] (right) projections.

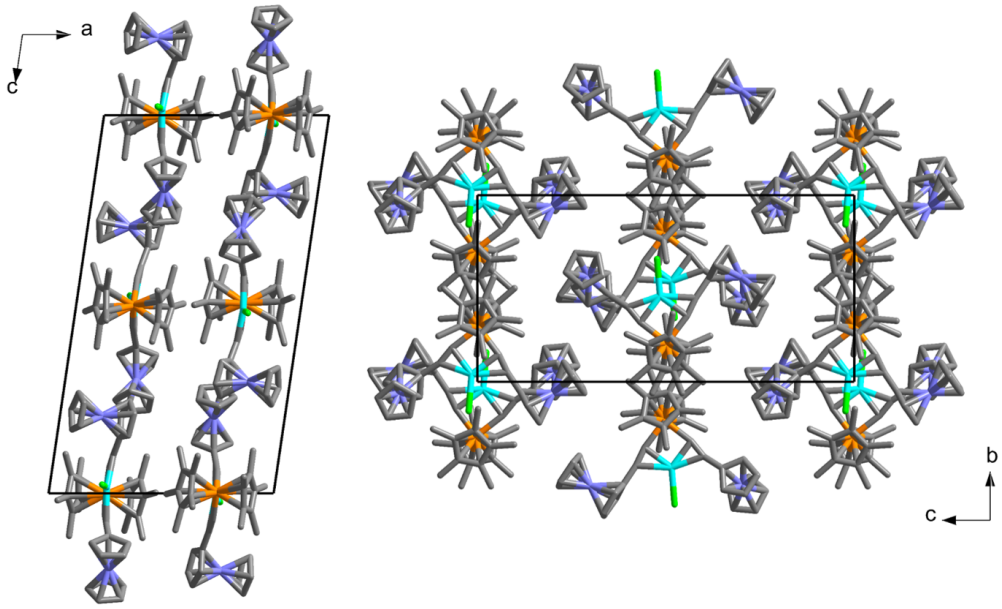

Figure S3: Packing arrangement in $Cp^*_2Ti(C_2Fc)_2$ along [100] (left) and [010] (right) projections.

`

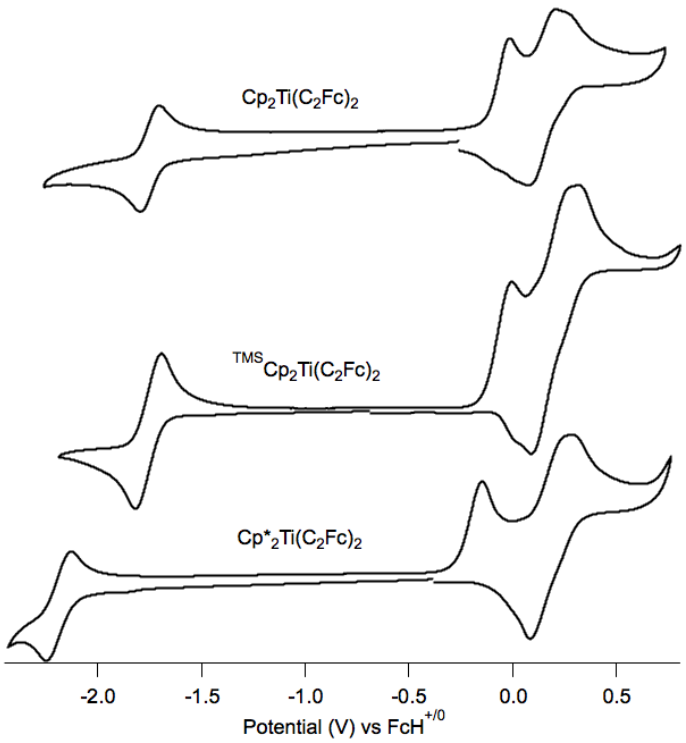

Figure S4: Cyclic voltammograms of $Cp_2Ti(C_2Fc)_2$, $^{TMS}Cp_2Ti(C_2Fc)_2$, and $Cp^*_2Ti(C_2Fc)_2$. Conditions: [Ti] ~ 1 mM in CH_2Cl_2 (0.1 M [*n*-Bu_4N][ClO_4]), glassy carbon working electrode, Ag^+/Ag reference electrode, and scan rate = 100 mV/s. The x-axis reports voltage vs FcH as determined by recording a voltammogram of FcH before and after data collection. Voltage sweeps are initiated in the cathodic direction.

`

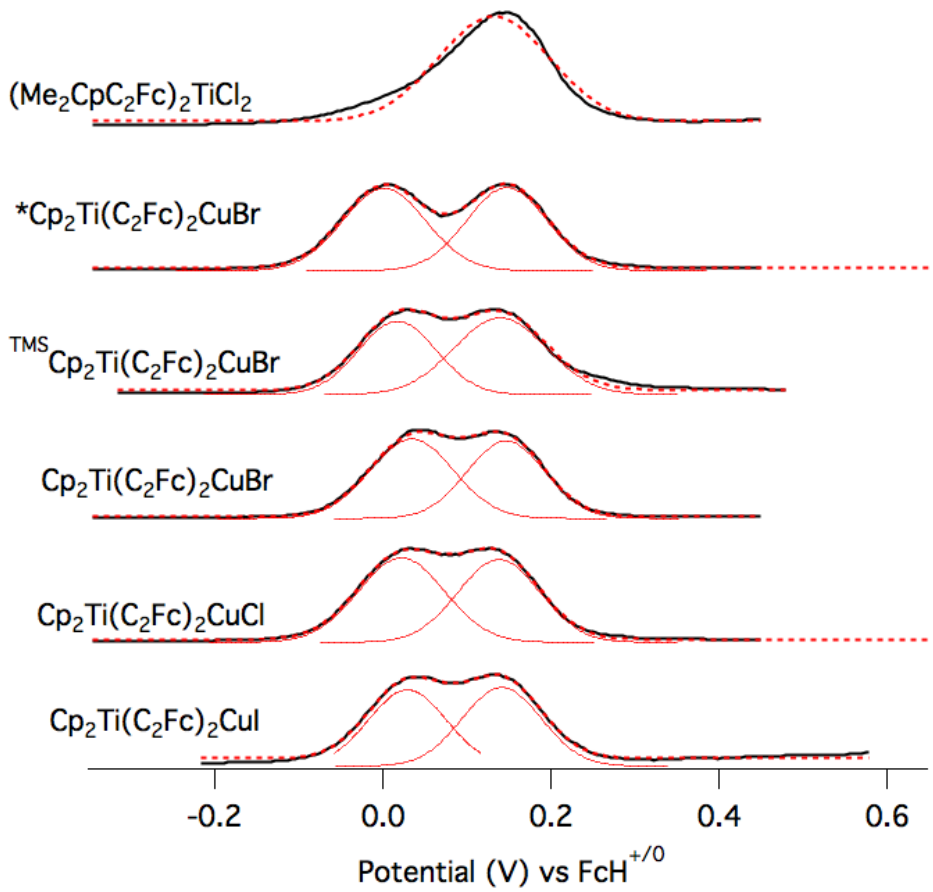

Figure S5: Differential Pulse voltammograms of $(Me_2CpC_2Fc)_2TiCl_2$, $Cp^*_2Ti(C_2Fc)_2CuBr$, $^{TMS}Cp_2Ti(C_2Fc)_2CuBr$, $Cp_2Ti(C_2Fc)_2CuBr$, $Cp2Ti(C_2Fc)_2CuCl$, $Cp2Ti(C_2Fc)_2CuI$, and. Conditions: [Ti] ~ 1 mM in CH_2Cl_2 (0.1 M [*n*-Bu_4N][PF_6]), glassy carbon working electrode, Ag^+/Ag reference electrode, step E = 4 mV, pulse width = 50 ms, pulse period = 200 ms, and pulse amplitude = 10 mV. The x-axis reports voltage vs FcH as determined by recording a voltammogram of FcH before and after data collection. Voltage sweeps are initiated in the anodic direction. Experimental data is in black, gaussian peaks are solid red, and the gaussian fits are the dashed red lines.

`

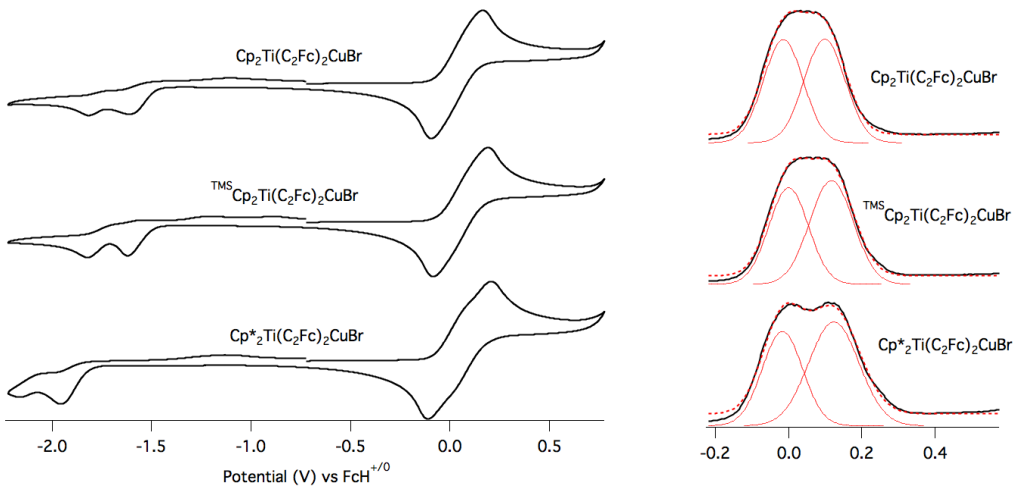

Figure S6: Differential Pulse Voltammograms and Cyclic Voltammograms of Cp2Ti(C_2Fc)$_2$CuBr, ^{TMS}Cp$_2$Ti(C_2Fc)$_2$CuBr, and Cp*$_2$Ti(C_2Fc)$_2$CuBr Conditions: [Ti] ~ 1 mM in THF (0.1 M [*n*-Bu$_4$N][PF$_6$]), glassy carbon working electrode, Ag$^+$/Ag reference electrode. Cyclic Voltammetry scan rate = 100 mV/s. Differential Pulse Voltammetry step E = 4 mV, pulse width = 50 ms, pulse period = 200 ms, and pulse amplitude = 10 mV. The x-axis reports voltage vs FcH as determined by recording a voltammogram of FcH before and after data collection. Voltage sweeps are initiated in the anodic direction. Experimental data is in black, gaussian peaks are solid red, and the gaussian fits are the dashed red lines.

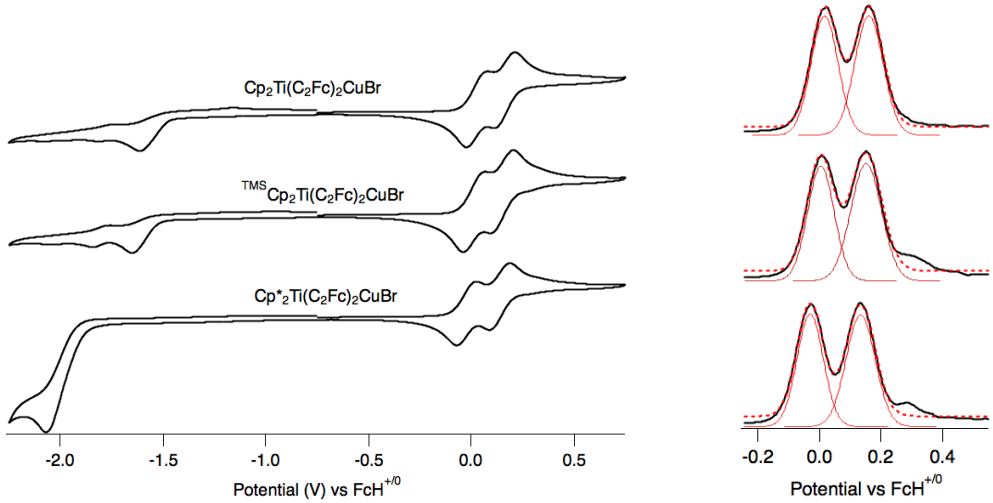

Figure S7: Differential Pulse Voltammograms and Cyclic Voltammograms of Cp2Ti(C_2Fc)$_2$CuBr, ^{TMS}Cp$_2$Ti(C_2Fc)$_2$CuBr, and Cp*$_2$Ti(C_2Fc)$_2$CuBr Conditions: [Ti] ~ 1 mM in CH_2Cl_2 (0.1 M [*n*-Bu$_4$N][B(C_6F_5)$_4$]), glassy carbon working electrode, Ag$^+$/Ag reference electrode. Cyclic Voltammetry scan rate = 100 mV/s. Differential Pulse Voltammetry step E = 4 mV, pulse width = 50 ms, pulse period = 200 ms, and pulse amplitude = 10 mV. The x-axis reports voltage vs FcH as determined by recording a voltammogram of FcH before and after data collection. Voltage sweeps are initiated in the anodic direction. Experimental data is in black, gaussian peaks are solid red, and the gaussian fits are the dashed red lines.

`

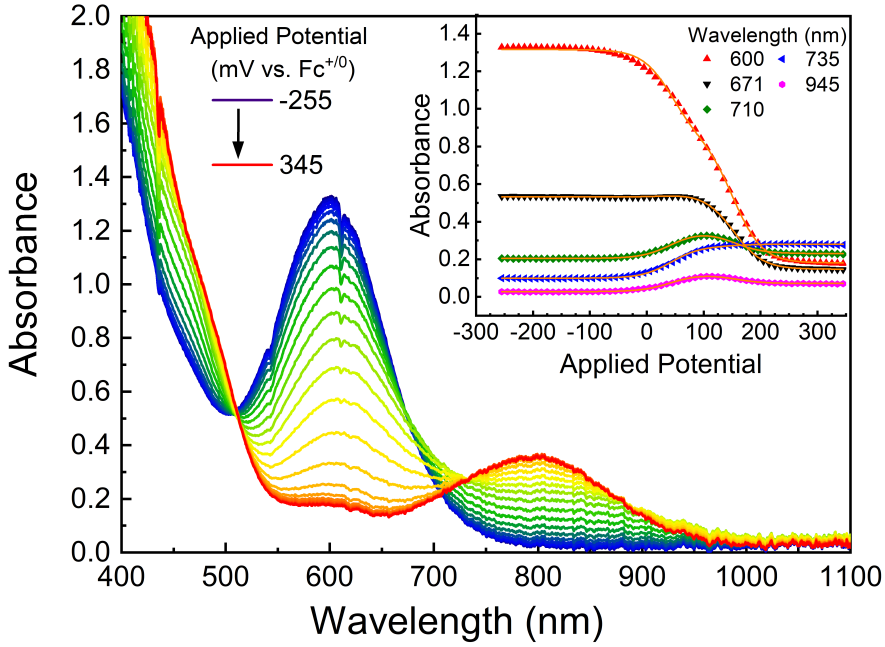

Figure S8: Spectroelectrochemical data for $Cp_2Ti(C_2Fc)_2CuBr$. Fitted single wavelength data (inset).

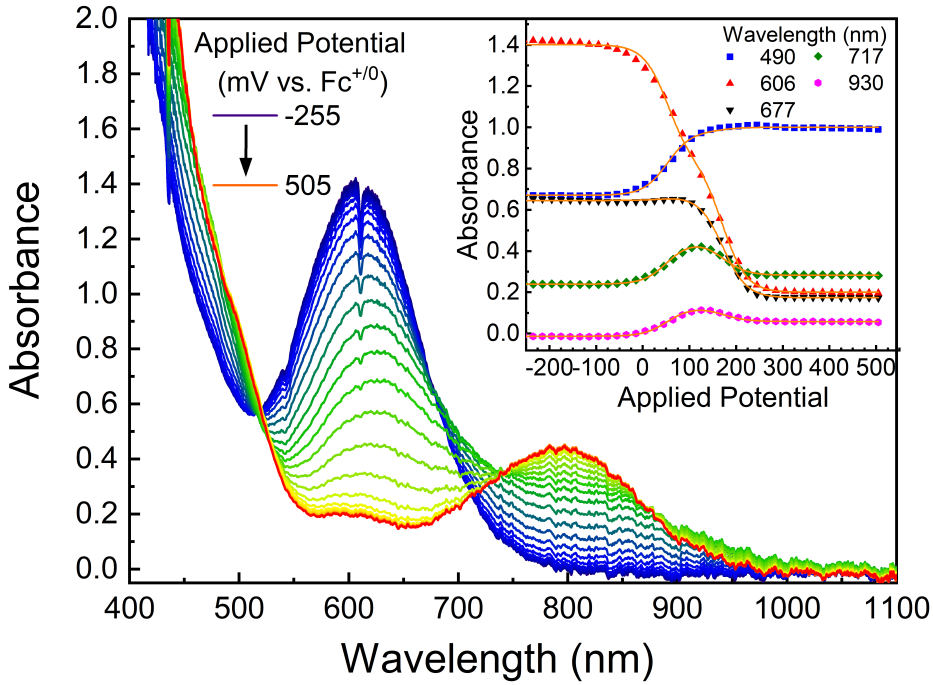

Figure S9: Spectroelectrochemical data for $^{TMS}Cp_2Ti(C_2Fc)_2CuBr$. Fitted single wavelength data (inset).

`

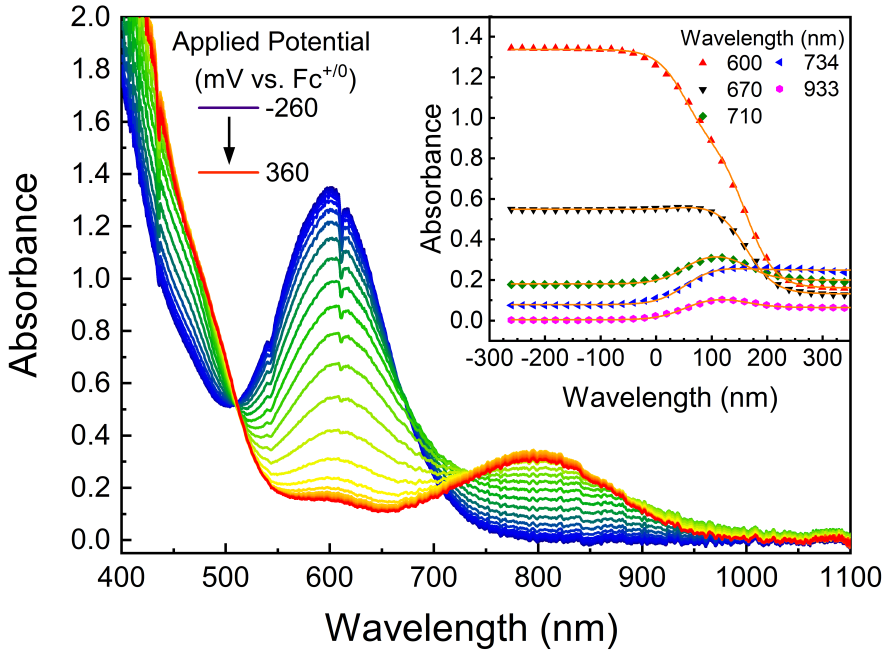

Figure S10: Spectroelectrochemical data for $Cp_2Ti(C_2Fc)_2CuCl$. Fitted single wavelength data (inset).

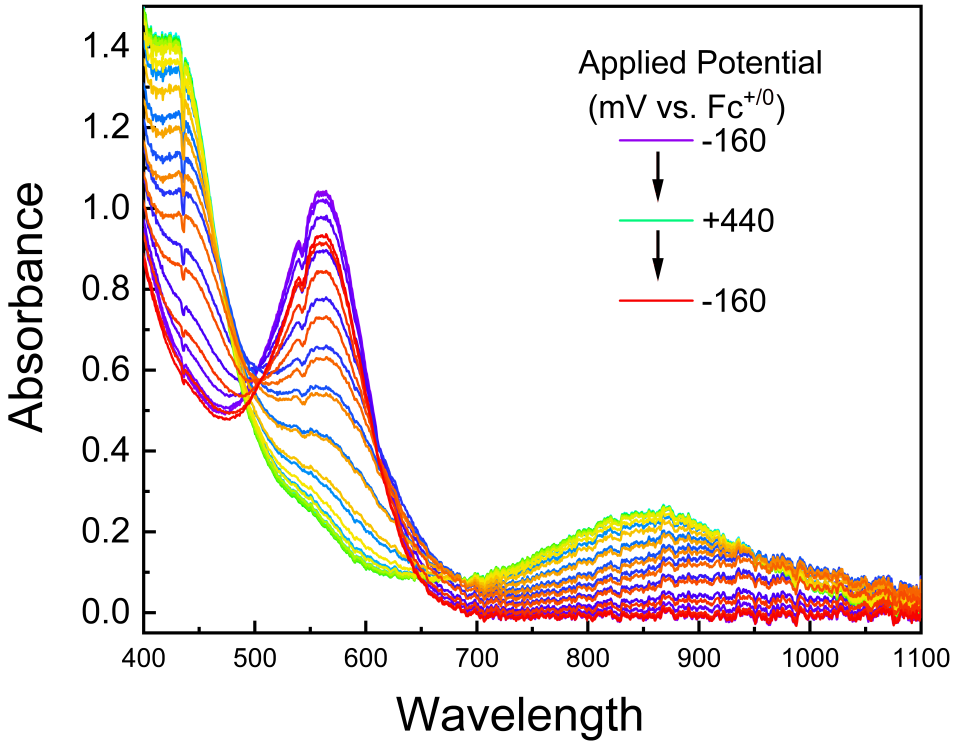

Figure S11: Spectroelectrochemical data for $Cp^*_2Ti(C_2Fc)_2CuBr$ for both the forward and return scan with some spectra removed for clarity. The starting spectrum is shown in purple, the spectrum at the most positive potential is shown in green, and the spectrum at the starting potential showing substantial reversibility is shown in red.

`

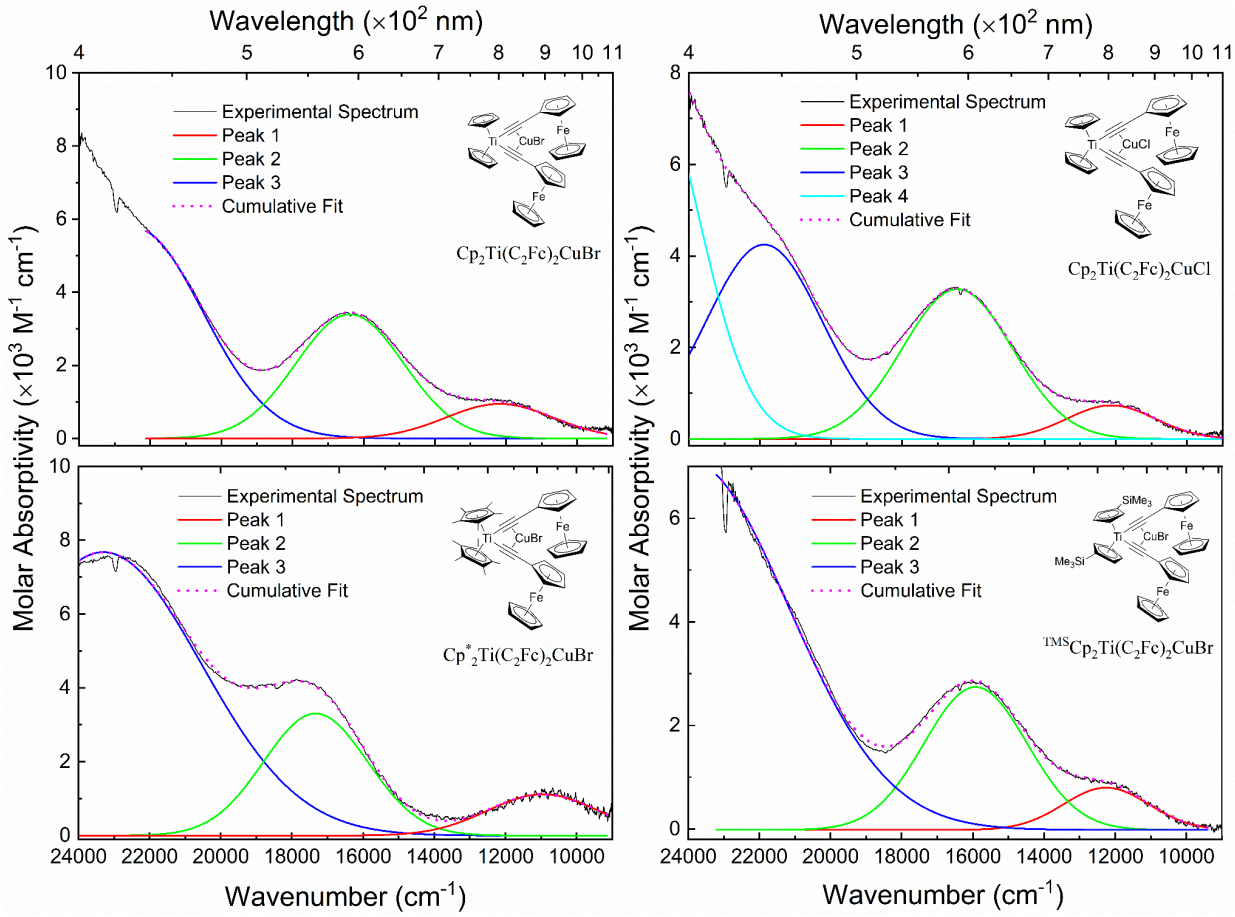

Figure S12: Gaussian fits of the spectra of the MV states for $Cp_2Ti(C_2Fc)_2CuBr$ (top left), $Cp_2Ti(C_2Fc)_2CuCl$ (top right), $Cp^*_2Ti(C_2Fc)_2CuBr$ (bottom left), and $^{TMS}Cp_2Ti(C_2Fc)_2CuBr$ (bottom right). Fits were performed with the x-axis in wavenumbers.

`

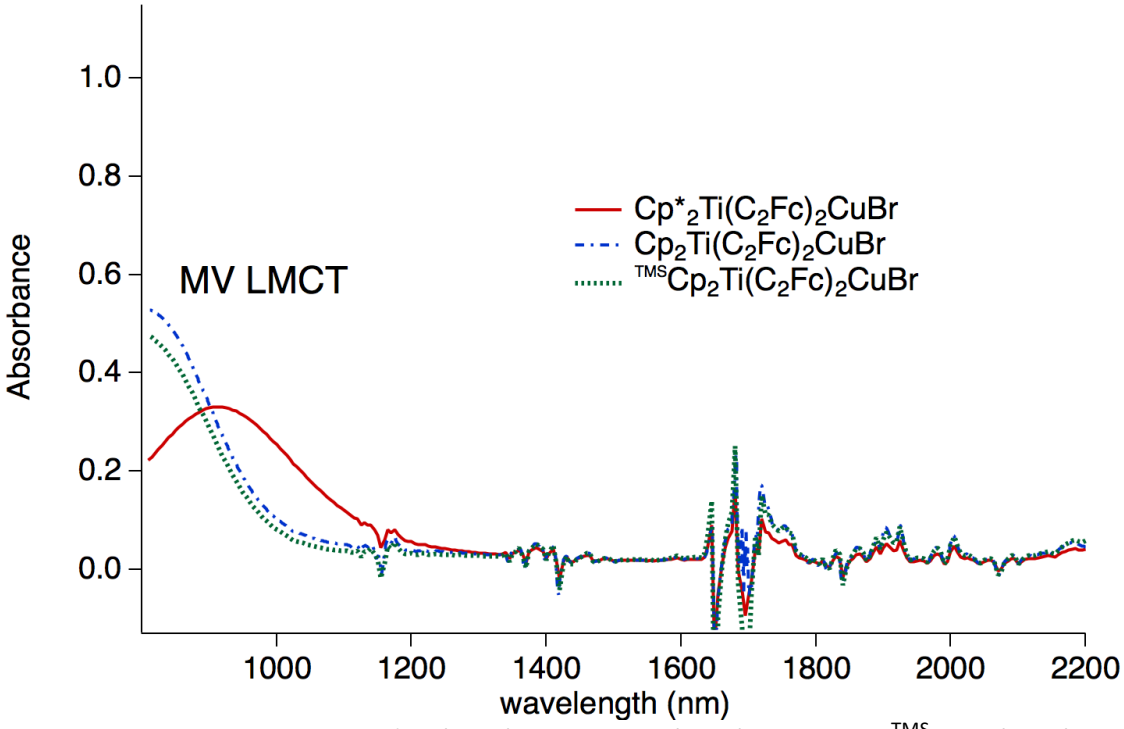

Figure S13: NIR spectra of $Cp^*_2Ti(C_2Fc)_2CuBr$, $Cp_2Ti(C_2Fc)_2CuBr$, and $^{TMS}Cp_2Ti(C_2Fc)_2CuBr$ in CH_2Cl_2 after the addition of 1 equivalent of $Cu(ClO_4)_2 \bullet 6H_2O$ (in CH_3CN). The highest energy NIR peaks are due to the MV species and were also observed in the spectroelectrochemical experiments. The higher amplitude noise at 1700 nm is due to the strong absorbance of CH_2Cl_2 at this wavelength. The smaller amplitude noise spikes coincide with CH_3CN absorbances.

`

Table S2: Coordinates for $Cp_2Ti(C_2Fc)_2CuBr$ obtained following optimization with the ωB97XD/Def2-TZV functional/basis.

Charge = 0 Multiplicity = 1

Cu -0.01438626 0.49622738 -0.93518228
Br 0.12074713 -1.33191229 -2.47204119
Ti -0.12417006 3.12907807 0.33490872
Fe -3.54376401 -1.86112837 0.35783330
Fe 3.65073644 -1.66088756 0.36751171
C -1.56601100 1.73013294 -0.20805599
C -2.37826437 0.84711169 -0.49029138
C -3.45174650 -0.06957780 -0.66187833
C -4.62516882 -0.11835492 0.17408686
H -4.85259655 0.56680334 0.97107452
C -5.42026779 -1.21820574 -0.25826483
H -6.36204782 -1.51804748 0.16559659
C -4.74358727 -1.86114947 -1.33939773
H -5.08558518 -2.73222828 -1.86919492
C -3.53208294 -1.15829761 -1.59283228
H -2.78045539 -1.40158496 -2.32206510
C -1.95429480 -1.88762652 1.67254039
H -1.31389789 -1.04093302 1.84904980
C -3.16718083 -2.17738588 2.36873565
H -3.58524784 -1.60376380 3.17691829
C -3.73743362 -3.35234203 1.78857376
H -4.66033509 -3.81902332 2.08444565
C -2.87409105 -3.78796357 0.73655390
H -3.03476021 -4.63810724 0.09756967
C -1.77184372 -2.88236732 0.66398475
H -0.96504605 -2.91774751 -0.04682915
C 1.42726144 1.84183621 -0.17245710
C 2.32629857 1.02645449 -0.38518968
C 3.47921066 0.20493324 -0.50077637
C 3.76183032 -0.77999452 -1.50573331
H 3.11641468 -1.02219738 -2.33077781
C 5.00635127 -1.38995670 -1.18129494
H 5.48626518 -2.17268343 -1.74115010
C 5.50399045 -0.79100641 0.01677261
H 6.42370983 -1.04241879 0.51414036
C 4.56145187 0.18306789 0.45208112
H 4.63768927 0.80994186 1.32246468
C 1.81503048 -2.12708669 1.18521839
H 0.94026211 -1.50885137 1.09019860

`

C 2.21242212 -3.14711724 0.27004164
H 1.68504239 -3.42029900 -0.62626176
C 3.44929638 -3.69294815 0.73136822
H 4.01599421 -4.46964496 0.24913925
C 3.81395160 -3.00995011 1.93246939
H 4.70129150 -3.18451048 2.51494264
C 2.80097931 -2.04132307 2.21474440
H 2.78973650 -1.36084444 3.04775303
C 1.07991257 3.10938705 2.39735126
C 0.28164411 4.27309618 2.38225128
H 0.63919171 5.28671044 2.38006517
C -1.08457052 3.87007362 2.36380222
H -1.93872523 4.52328499 2.35913988
C -1.12048842 2.45407054 2.40943536
H -2.00508375 1.84590500 2.41861753
C 0.21220895 1.98224543 2.39592241
H 0.52108622 0.95301413 2.39369763
C -1.36587251 4.39550026 -1.26961526
C -0.33933748 3.70337003 -1.96821752
H -0.48700757 2.93650156 -2.70722864
C 0.90777325 4.21484566 -1.53786657
H 1.87273022 3.89814561 -1.88588458
C 0.66134449 5.18005183 -0.53252520
H 1.40771136 5.74889659 -0.00807249
C -0.75198475 5.30347054 -0.38112162
H -1.25742540 5.97485867 0.28906843
H -2.42209298 4.22908031 -1.37718191
H 2.15430324 3.07681272 2.38303744

`

Table S3: Coordinates for $Cp_2Ti(C_2Fc)_2CuBr^+$ obtained following optimization with the B3LYP/6-31G(d) functional/basis.

Charge = 1 Multiplicity = 2

Ti 0.29074472 3.25370415 0.30191155
Cu -0.00725111 0.47537599 -0.64791841
Br -0.21595965 -1.54163736 -1.76907442
C -1.28887298 1.94519656 -0.02744575
C -2.00047304 0.97059695 -0.38356318
C -3.25465320 0.32398047 -0.60810304
Fe -3.93974198 -1.54208070 0.25991214
C -4.42121325 0.49678561 0.21345518
H -4.47601010 1.13026627 1.08849983
C -5.47405744 -0.29954419 -0.32386841
H -6.48128701 -0.36590150 0.06496427
C -4.95463881 -0.99786713 -1.45914931
H -5.49542403 -1.69666874 -2.08307020
C -3.59138332 -0.62397481 -1.62272920
H -2.89199553 -1.01797813 -2.34601267
C -2.40590209 -2.37879555 1.49159277
H -1.45281916 -1.88800671 1.63925122
C -3.59010254 -2.15353700 2.24455392
H -3.68353750 -1.49979173 3.10167661
C -4.64497443 -2.90845598 1.64465519
H -5.67142161 -2.94900748 1.98341724
C -4.09871416 -3.59850844 0.51564184
H -4.64075659 -4.24695408 -0.15952478
C -2.71528638 -3.26390816 0.42608871
H -2.03065894 -3.55704176 -0.35813444
C 1.56624929 1.71657461 -0.23346128
C 2.12567729 0.64379414 -0.56003025
C 3.21203139 -0.26550531 -0.76801568
Fe 3.65266460 -2.01648094 0.20321869
C 3.33247759 -1.34577751 -1.70857760
H 2.54012228 -1.69007517 -2.35599918
C 4.64390625 -1.88775207 -1.59449107
H 5.03196846 -2.72365790 -2.16183703
C 5.34772473 -1.15946437 -0.58724181
H 6.36304526 -1.34229436 -0.26006730
C 4.47127428 -0.16686969 -0.06537324
H 4.69752329 0.55336404 0.70946897
C 2.13867065 -2.35793404 1.53792495
H 1.30333640 -1.68426632 1.68019555

`

C 2.20222911 -3.41431931 0.57902144
H 1.42284184 -3.67084038 -0.12525725
C 3.49641144 -4.01160847 0.67018814
H 3.86461092 -4.82833589 0.06275271
C 4.23204747 -3.32260354 1.68243426
H 5.25250949 -3.52851223 1.97886668
C 3.39148455 -2.30043625 2.22130473
H 3.66387817 -1.59610313 2.99673225
C 1.62620554 3.10655786 2.29561032
C 1.13175097 4.42804491 2.20083935
H 1.72663816 5.32215885 2.07605565
C -0.28654022 4.37823782 2.32385184
H -0.95775421 5.22606020 2.31242416
C -0.66033804 3.02516304 2.50835982
H -1.66826031 2.65804351 2.63968225
C 0.51788706 2.23657598 2.47539164
H 0.56597704 1.15976208 2.55810288
H 2.66316945 2.80813219 2.22761172
C -0.94293088 4.43109769 -1.40025774
C 0.04117177 3.64920023 -2.06522679
H -0.15125976 2.82247877 -2.73513958
C 1.31801220 4.13753292 -1.69212135
H 2.26866548 3.75046954 -2.03004550
C 1.12861400 5.20142932 -0.77696442
H 1.91165085 5.79156770 -0.32094227
C -0.27400241 5.38753468 -0.60310170
H -0.74278199 6.14003764 0.01581107
H -2.01392667 4.30696399 -1.48285373

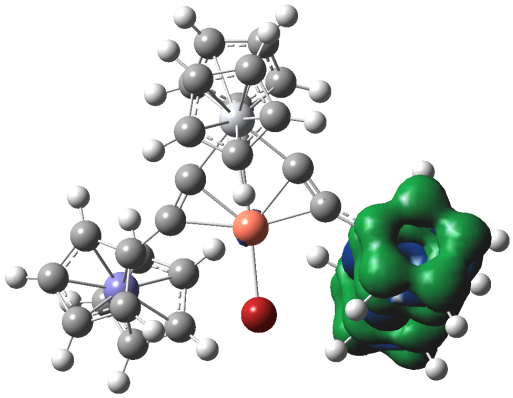

Figure S14: Electron Density from Spin SCF Density (isoval =0.0004). Coordinates used for the calculation listed in Table S3.

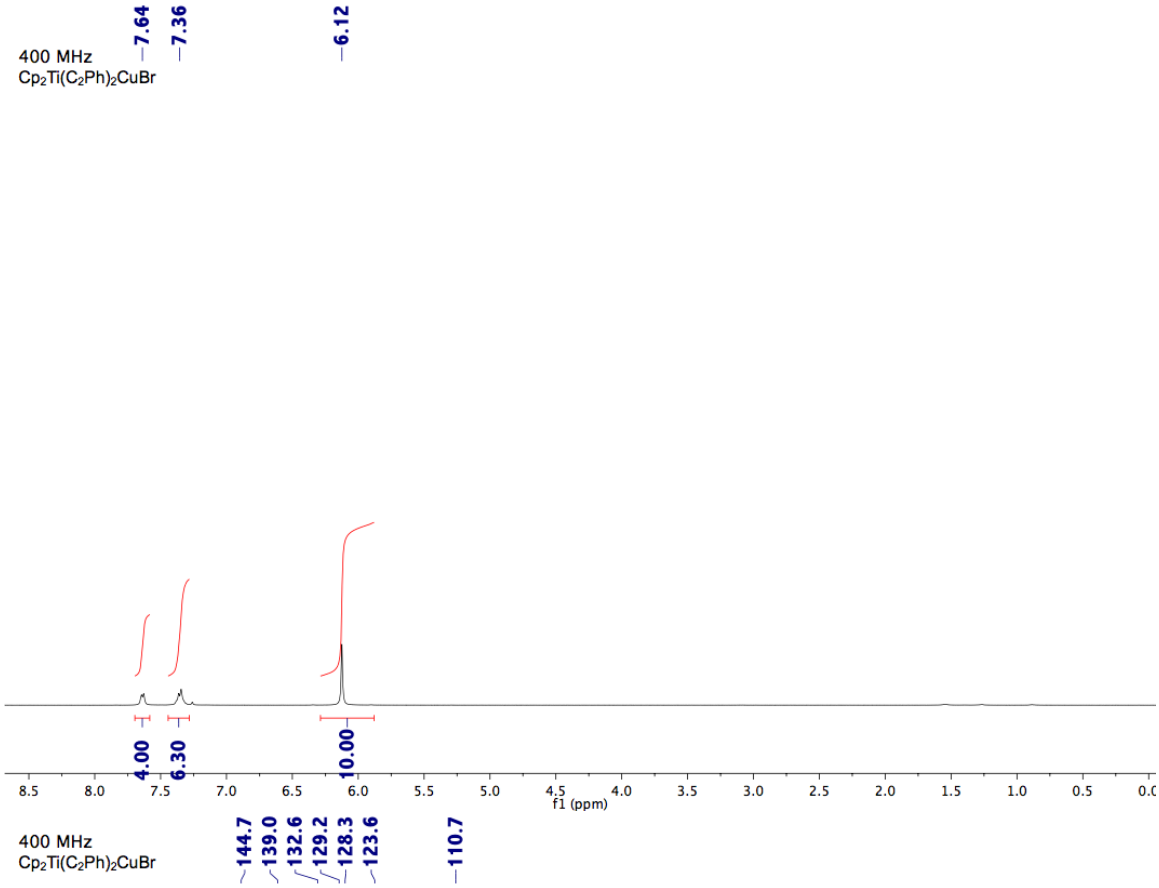

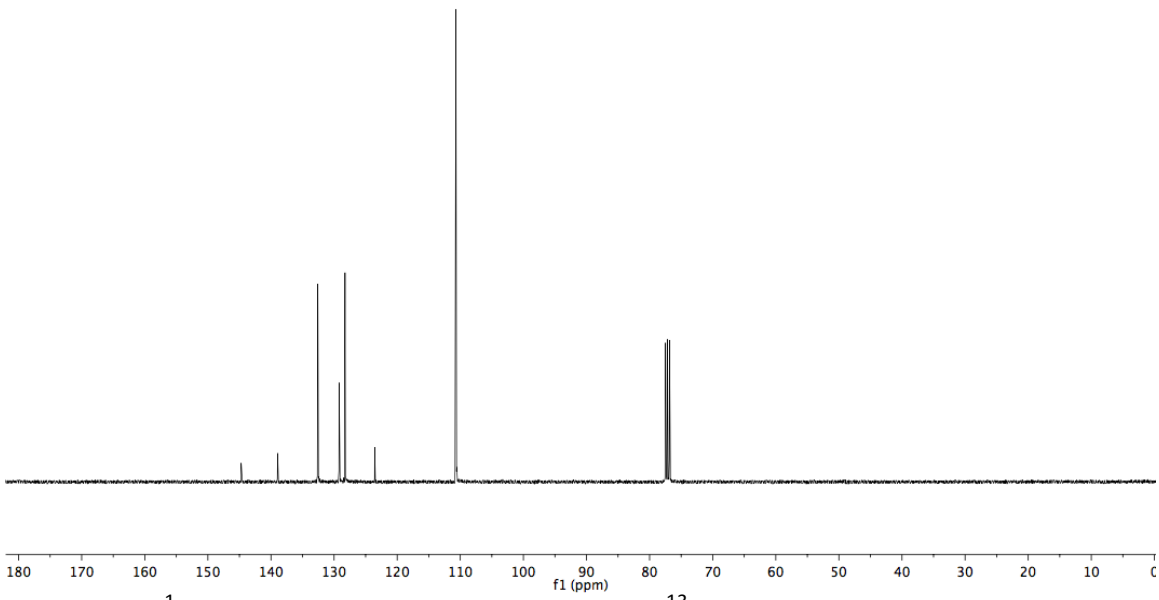

Figure S15: ^{1}H-NMR spectrum (400 MHz, top) and ^{13}C-NMR spectrum (400 MHz, bottom) of $Cp_2Ti(C_2Ph)_2CuBr$

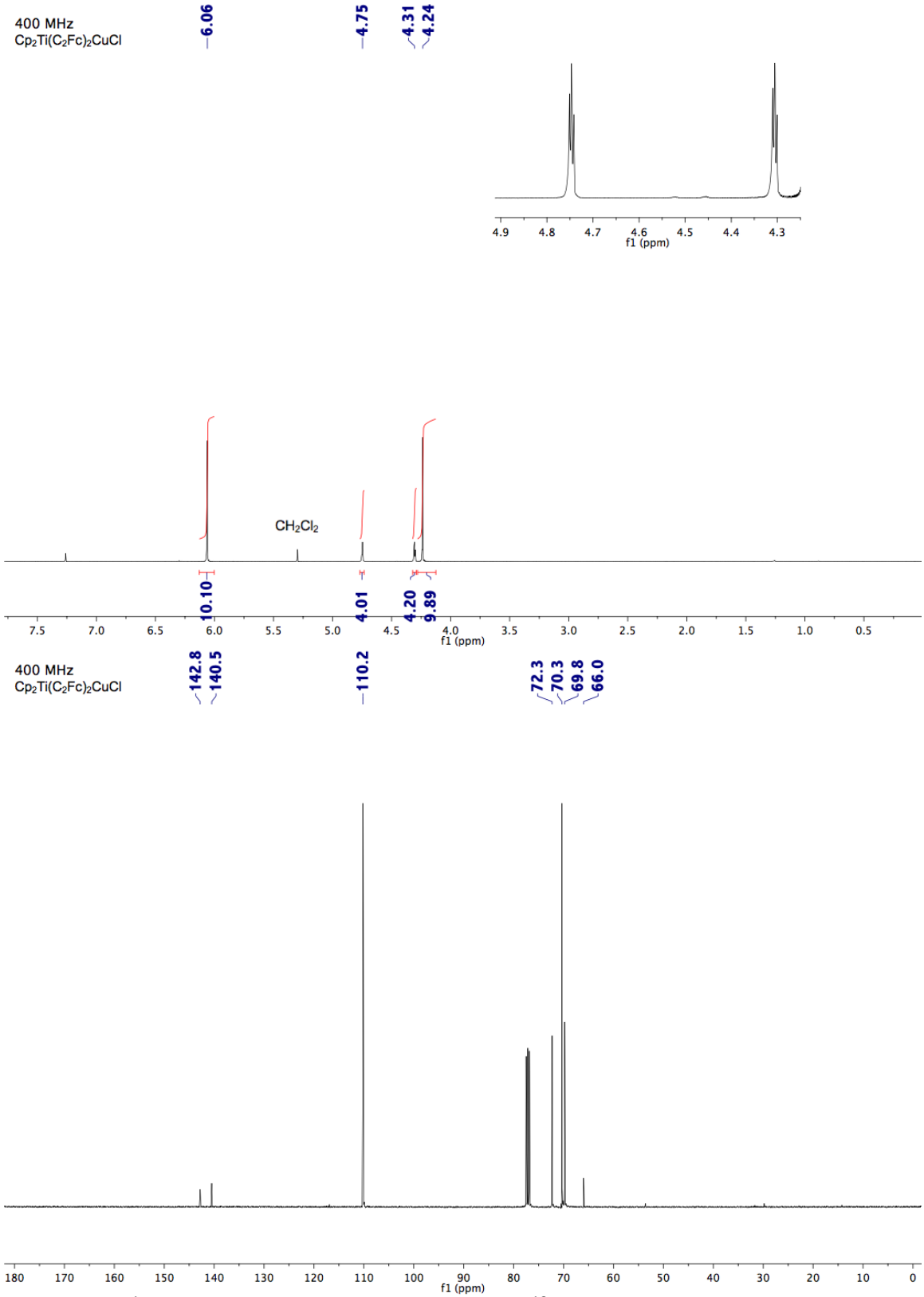

Figure S16: ^{1}H-NMR spectrum (400 MHz, top) and ^{13}C-NMR spectrum (400 MHz, bottom) of $Cp_2Ti(C_2Fc)_2CuCl$

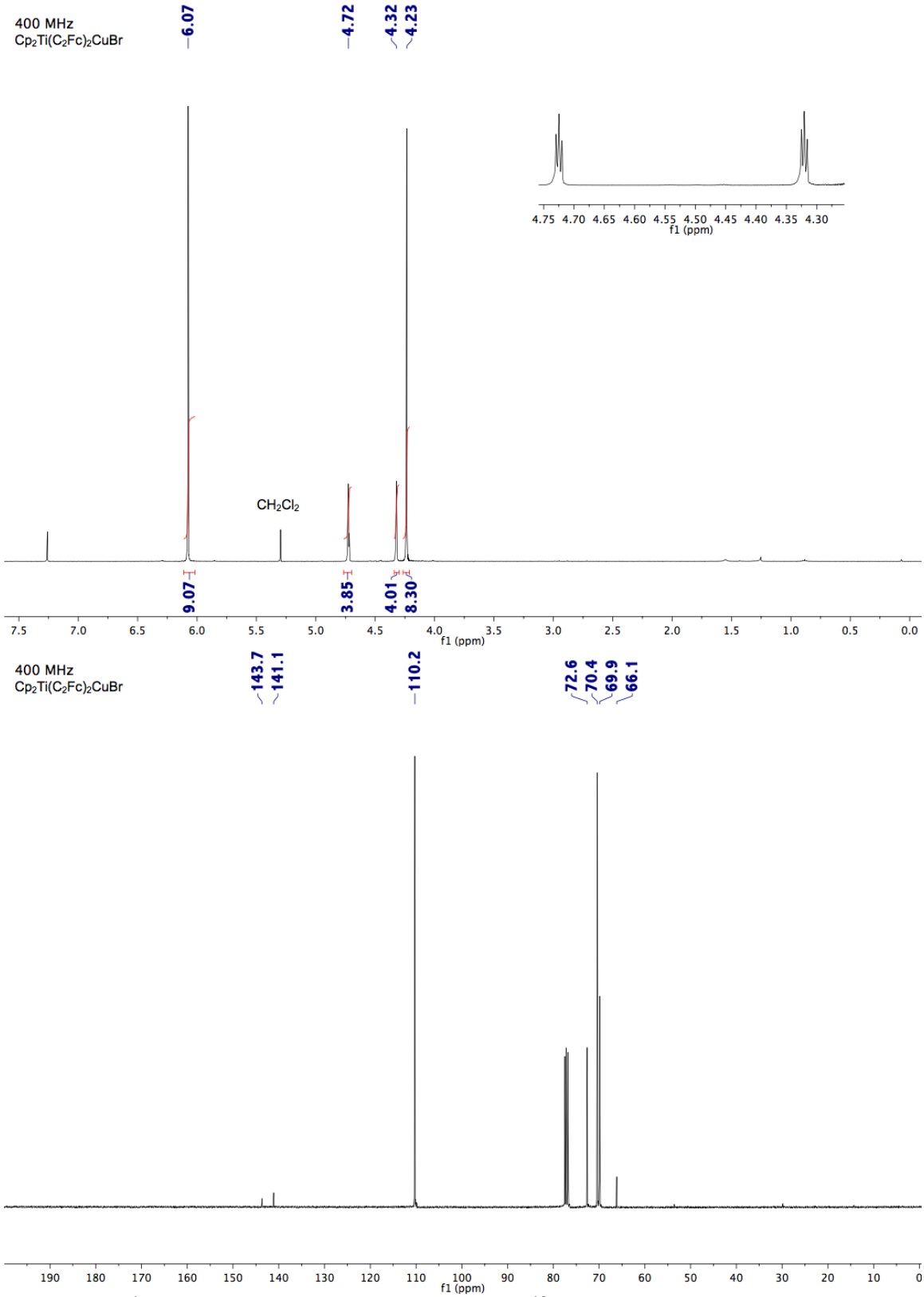

Figure S17: ^{1}H-NMR spectrum (400 MHz, top) and ^{13}C-NMR spectrum (400 MHz, bottom) of $Cp_2Ti(C_2Fc)_2CuBr$

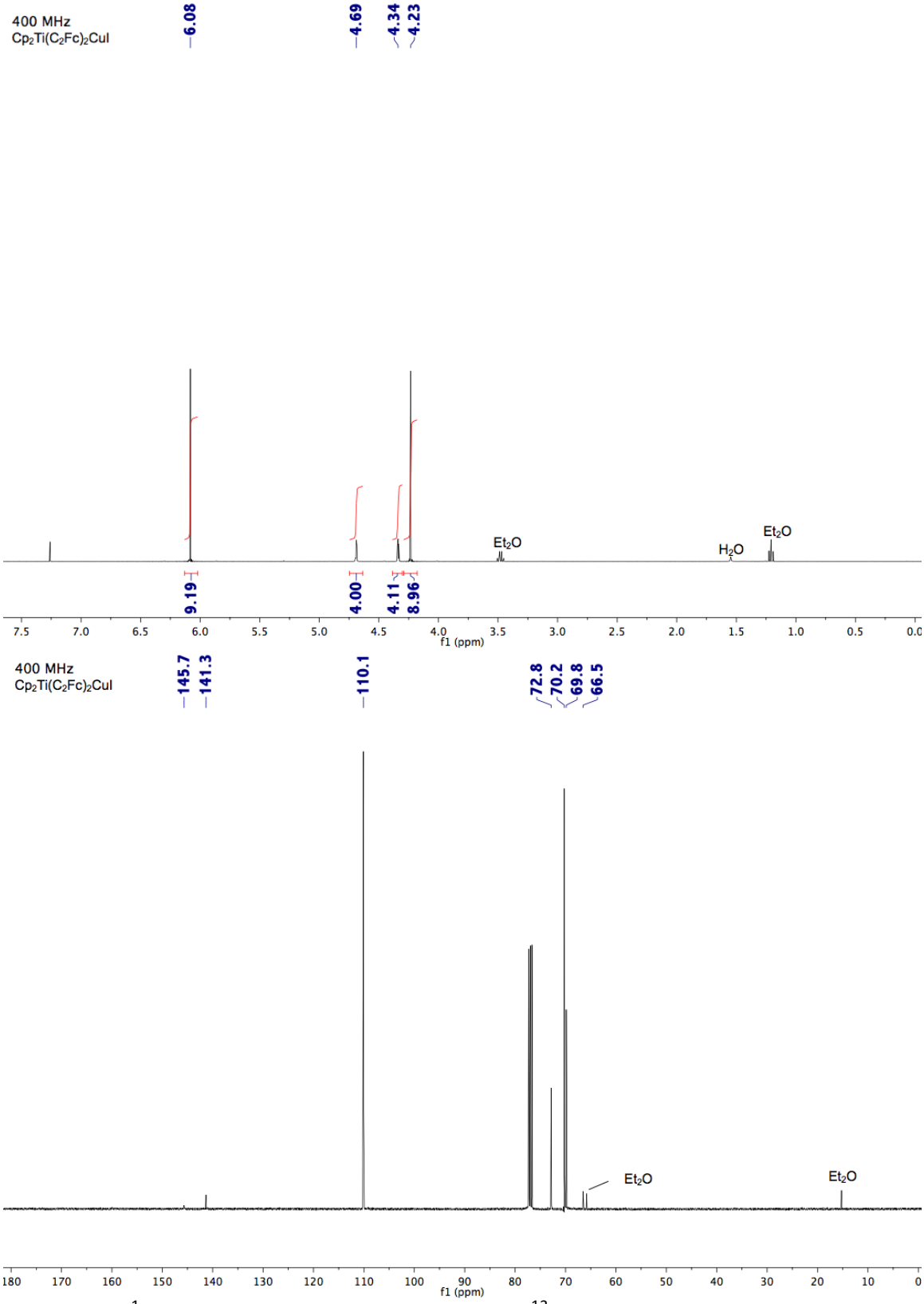

Figure S18: ^{1}H-NMR spectrum (400 MHz, top) and ^{13}C-NMR spectrum (400 MHz, bottom) of $Cp_2Ti(C_2Fc)_2CuI$

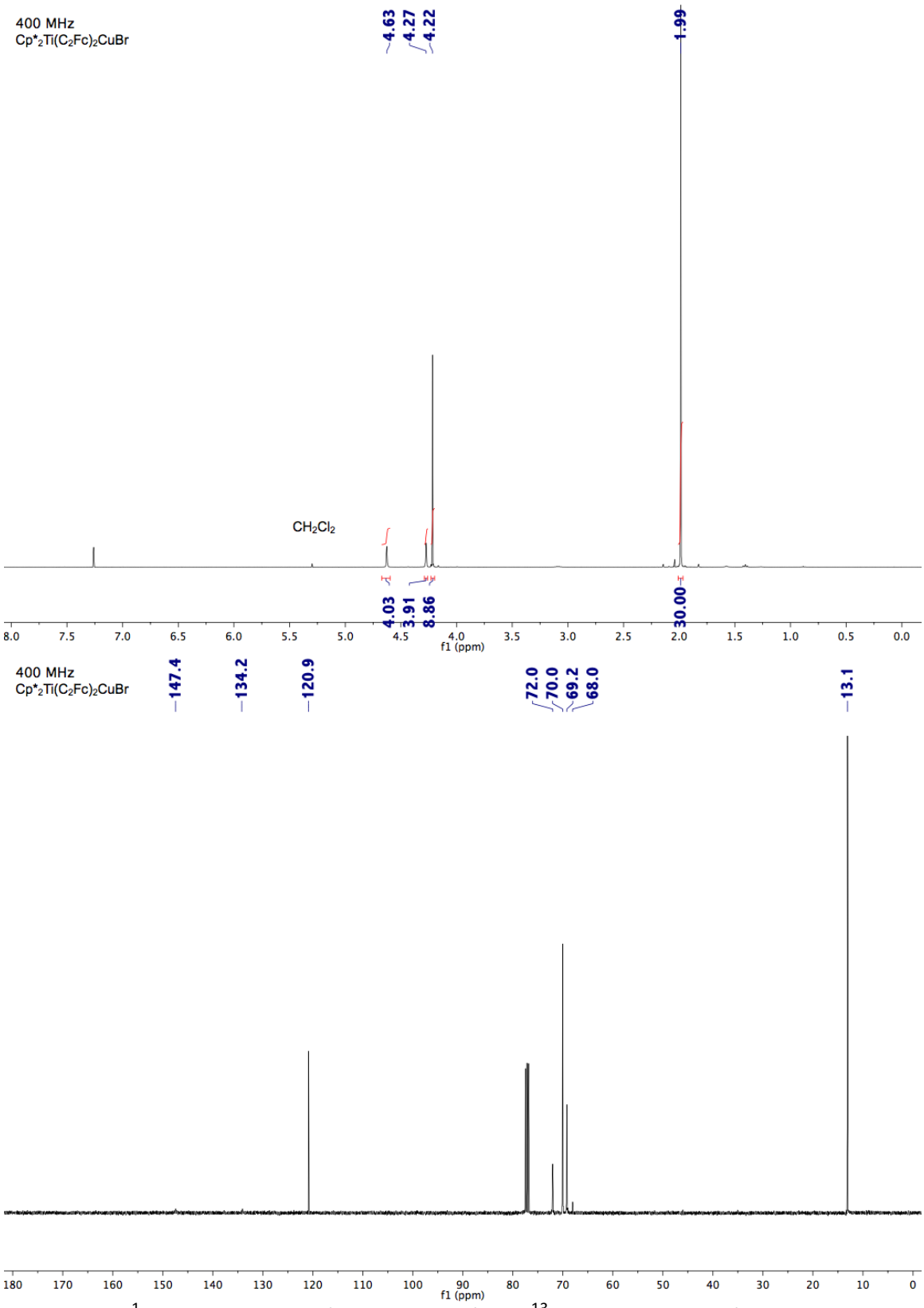

Figure S19: ^{1}H-NMR spectrum (400 MHz, top) and ^{13}C-NMR spectrum (400 MHz, bottom) of $Cp^*_2Ti(C_2Fc)_2CuBr$

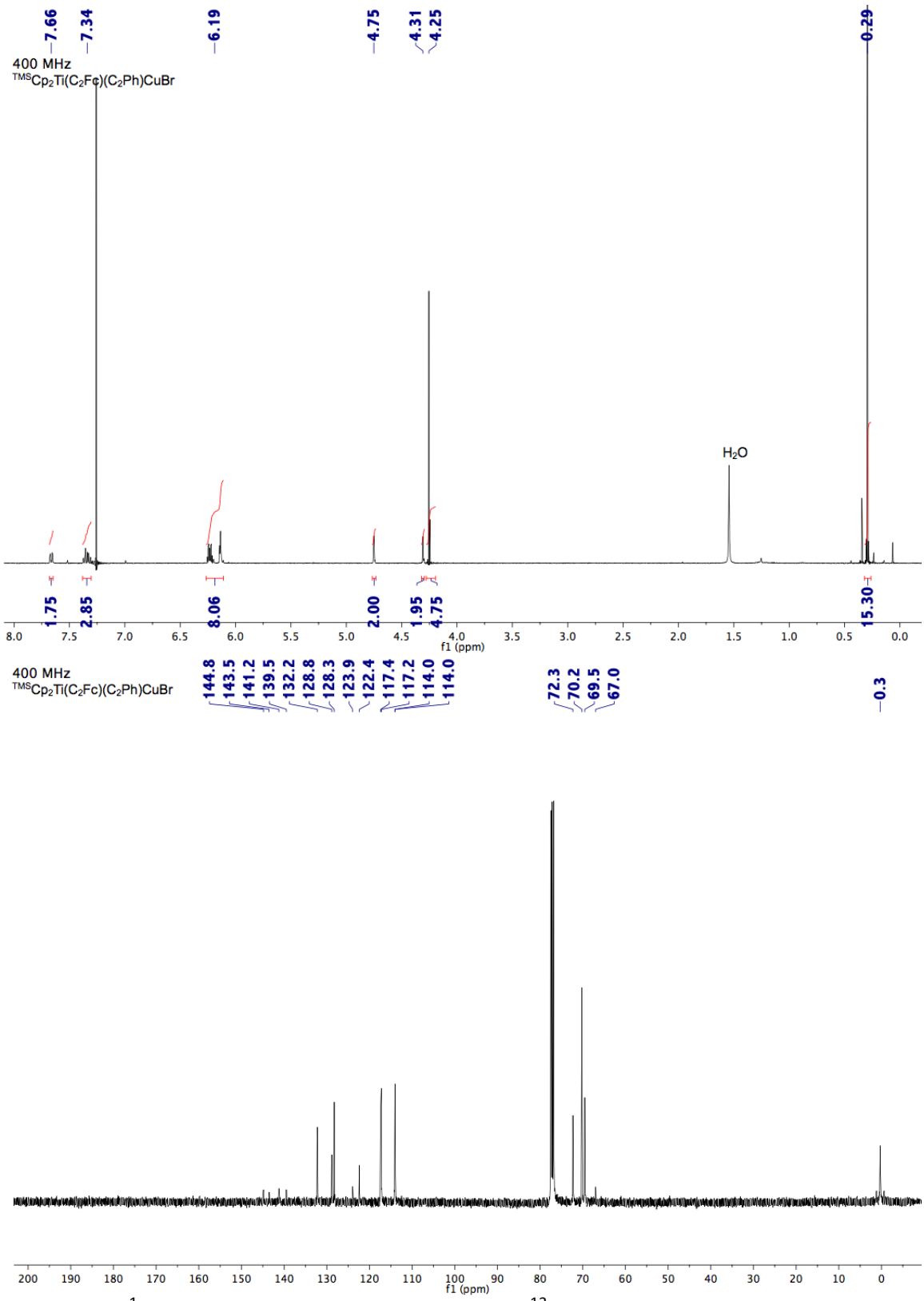

Figure S20: ^{1}H-NMR spectrum (400 MHz, top) and ^{13}C-NMR spectrum (400 MHz, bottom) of $^{TMS}Cp_2Ti(C_2Fc)(C_2Ph)CuBr$

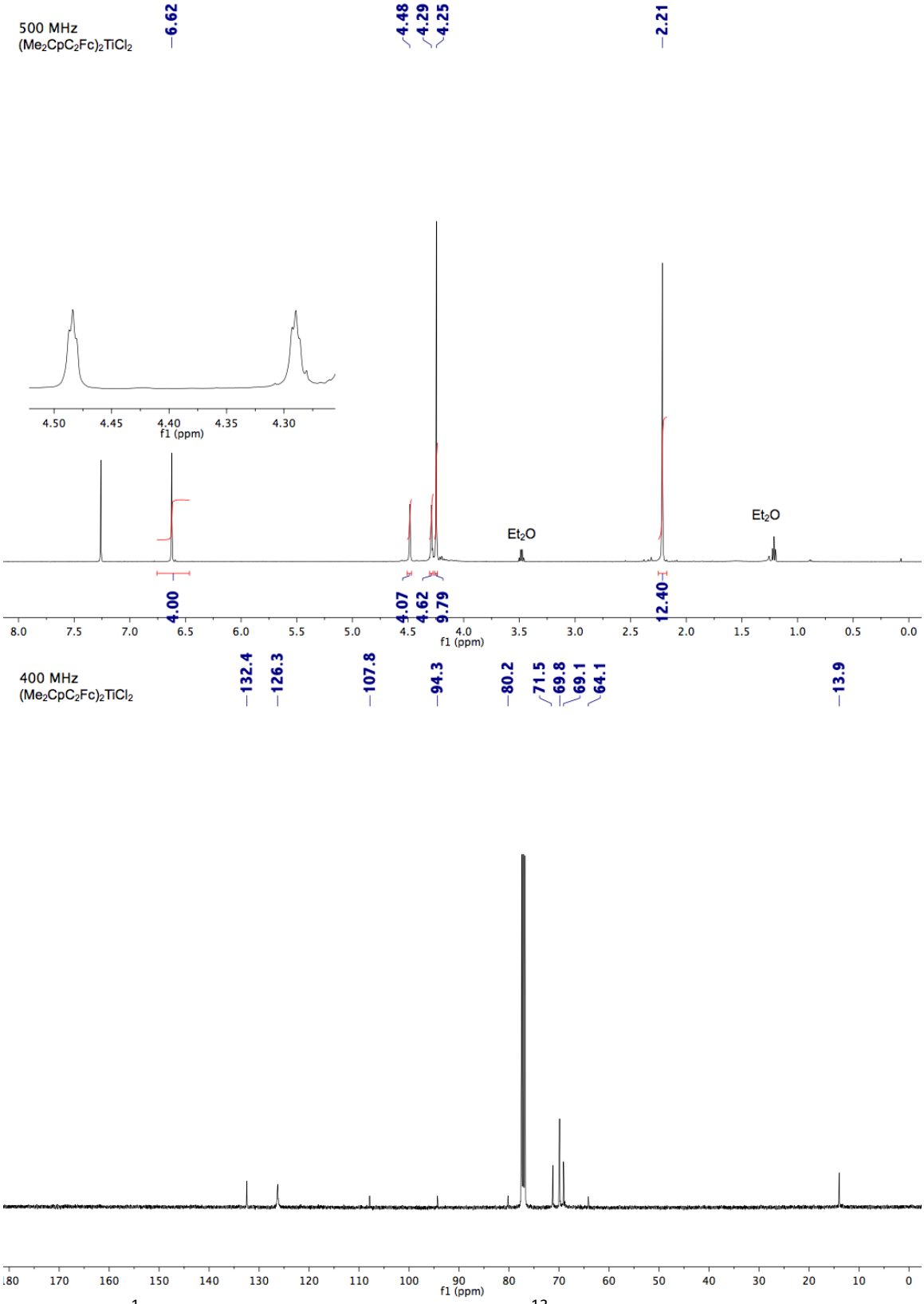

Figure S21: ^{1}H-NMR spectrum (500 MHz, top) and ^{13}C-NMR spectrum (400 MHz, bottom) of $(Me_2CpC_2Fc)_2TiCl_2$

`

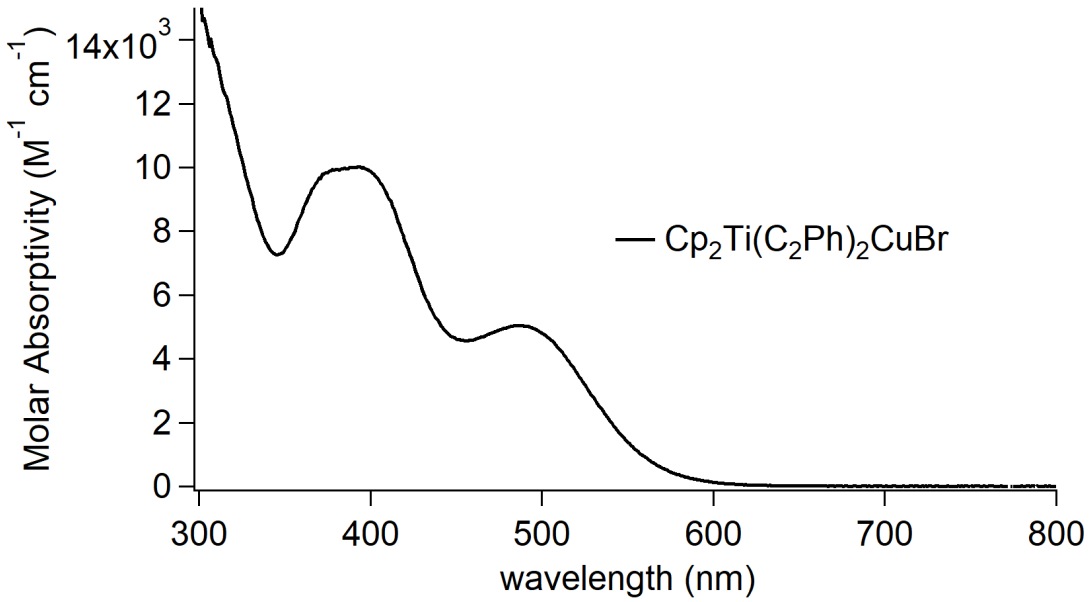

Figure S22: UV-Visible Spectrum of $Cp_2Ti(C_2Ph)_2CuBr$ in CH_2Cl_2.

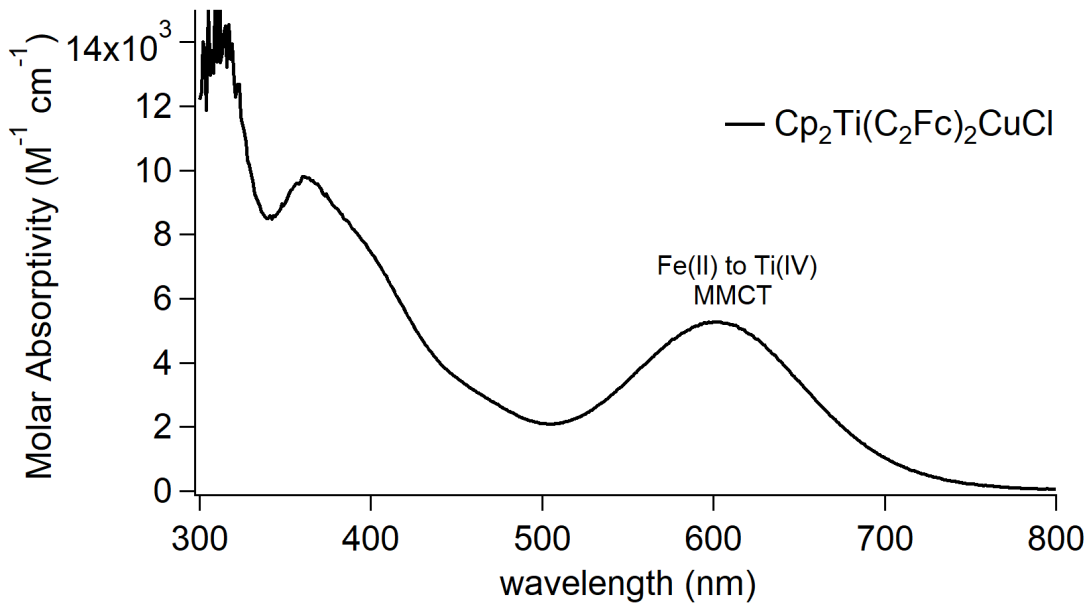

Figure S23: UV-Visible Spectrum of $Cp_2Ti(C_2Fc)_2CuCl$ in CH_2Cl_2.

`

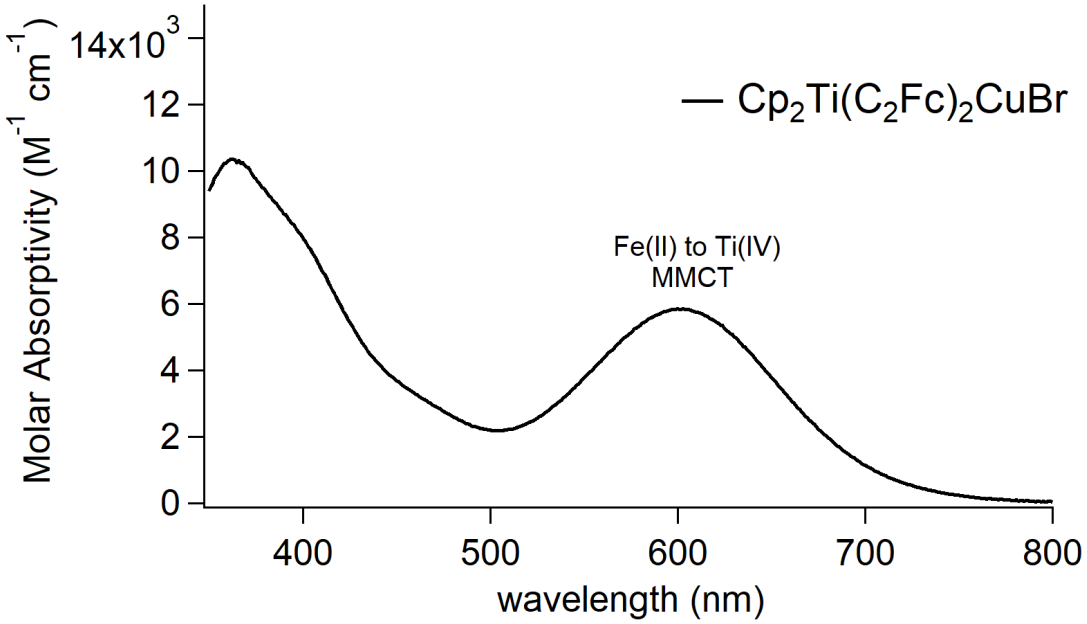

Figure S24: UV-Visible Spectrum of $Cp_2Ti(C_2Fc)_2CuBr$ in CH_2Cl_2.

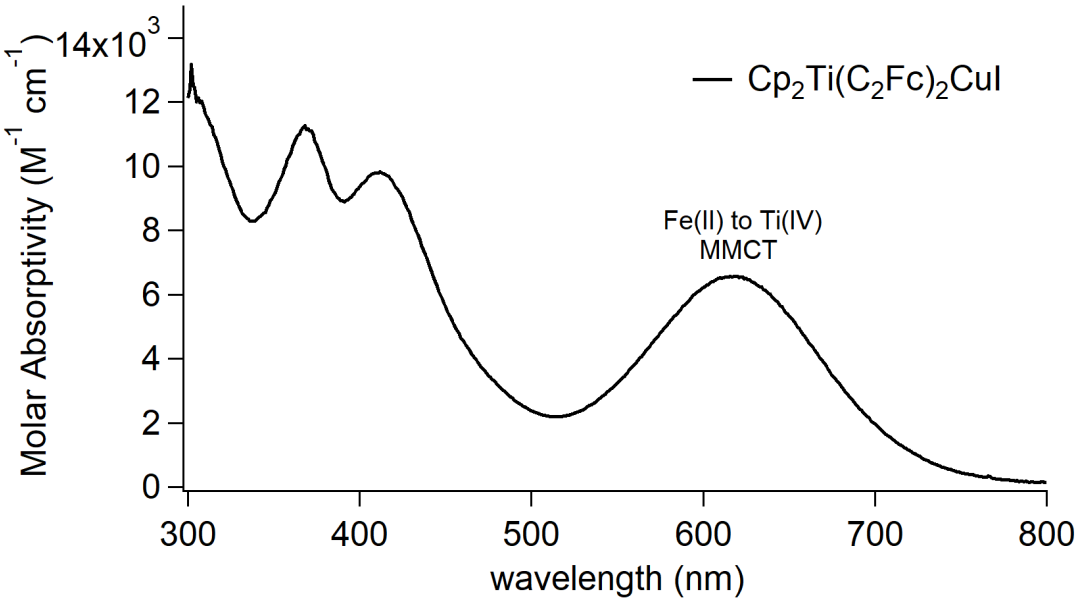

Figure S25: UV-Visible Spectrum of $Cp_2Ti(C_2Fc)_2CuI$ in CH_2Cl_2.

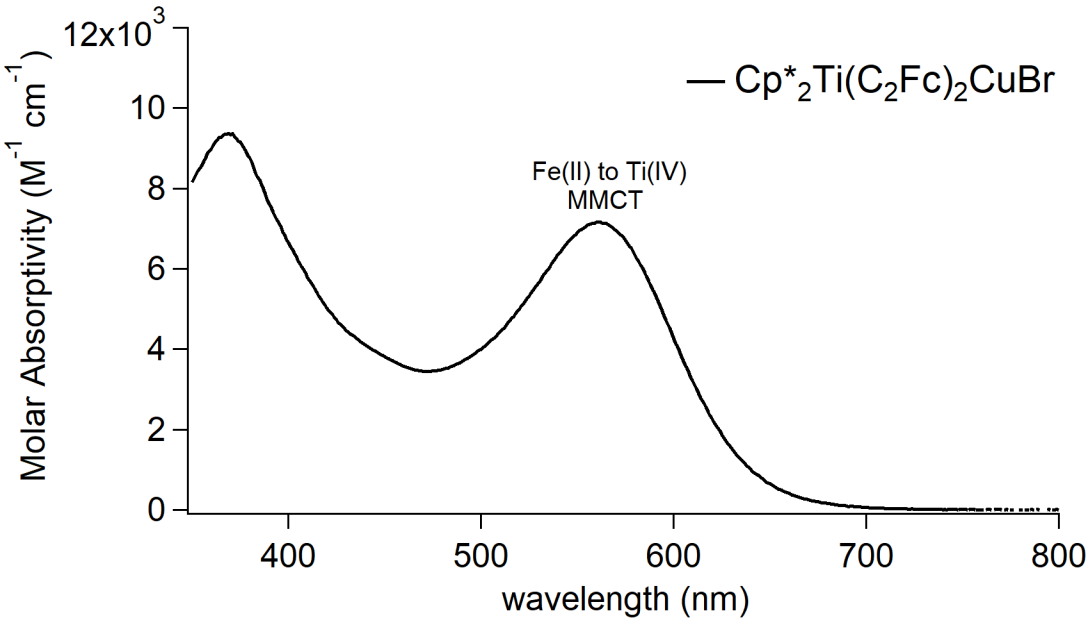

Figure S26. UV-Visible Spectrum of $Cp^*_2Ti(C_2Fc)_2CuBr$ in CH_2Cl_2.

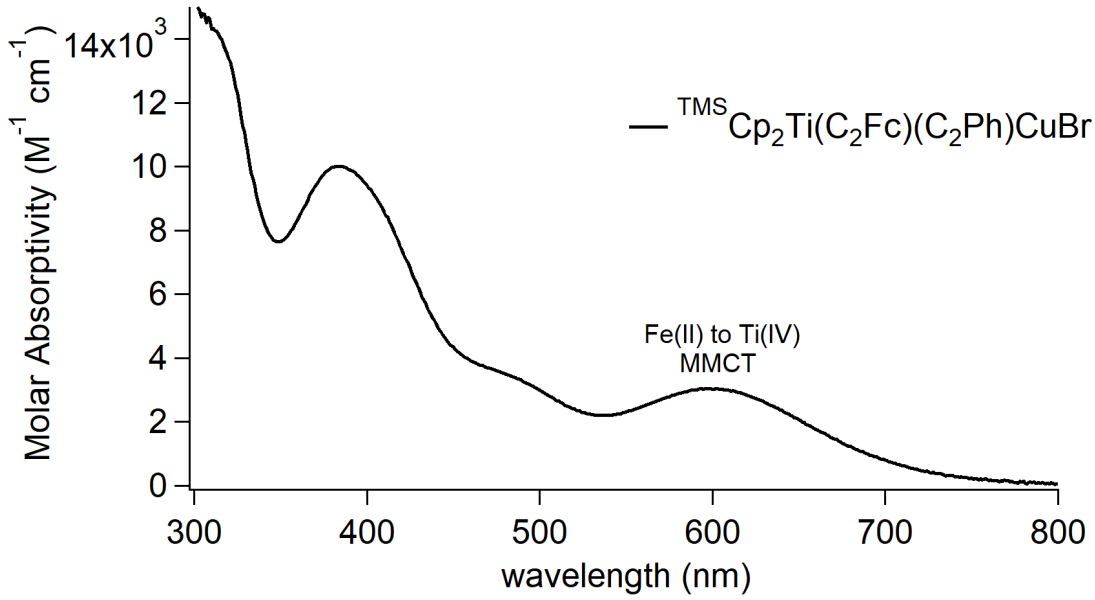

Figure S27: UV-Visible Spectrum of $^{TMS}Cp_2Ti(C_2Fc)(C_2Ph)CuBr$ in CH_2Cl_2.

`

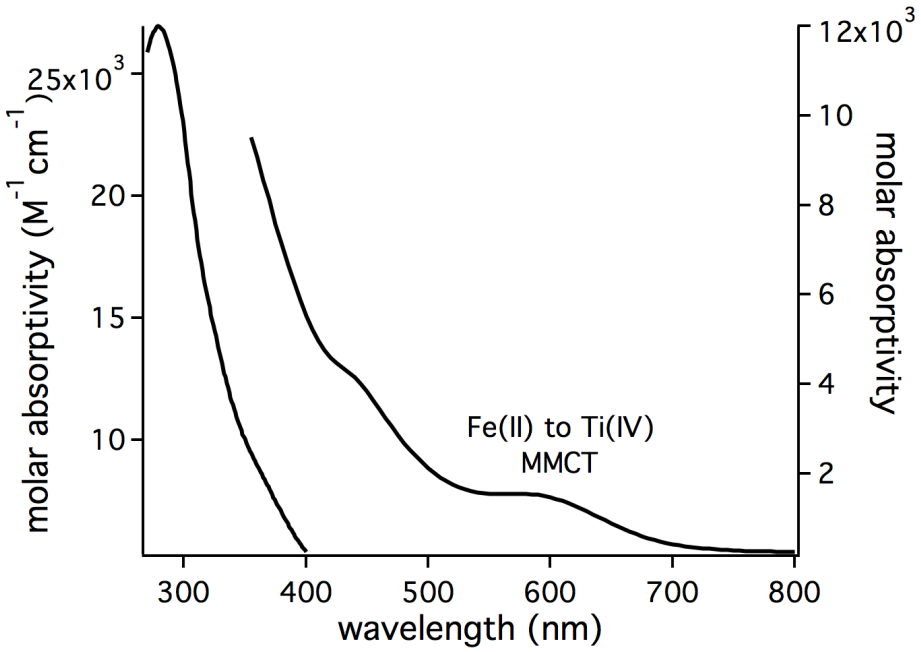

Figure S28: UV-Visible Spectrum of $(Me_2CpC_2Fc)_2TiCl_2$ in CH_2Cl_2.